JOURNAL OF GEOPHYSICAL RESEARCH, VOL. 102, NO. D6, PAGES 6637–6653, MARCH 27, 1997

A modeling and observational study of the detailed microphysical structure of tropical cirrus anvils

Jen-Ping Chen
Department of Atmospheric Sciences, National Taiwan University, Taipei, Taiwan, R. O. C.

Greg M. McFarquhar and Andrew J. Heymsfield
National Center for Atmospheric Research, Boulder, Colorado

V. Ramanathan
Center for Clouds, Chemistry and Climate, Scripps Institution of Oceanography, La Jolla, California

Abstract. A detailed microphysical analysis of ice particles in a cirrus anvil is presented, using a combination of observational data and model simulations for missions flown during the Central Equatorial Pacific Experiment (CEPEX). The observational data are obtained mainly from the two-dimensional cloud probe, measuring particles as small as 100 μm in diameter; the model simulations are done with a detailed microphysical model that categorizes cloud particles according to their size, shape, and solute content. Detailed analyses of the simulated particle size spectra are made for the size range of 1 μm to several millimeters, which are then compared with the observational results. The evolution of the cirrus anvil is divided into four stages: the deep convection, the precipitating anvil, the extended anvil and the detached anvil. Discussions on the properties of the simulated cloud systems are given in detail for each stage. Model results show that the number concentration of ice particles in the anvils can reach over 1000 per liter. Frozen cloud droplets and interstitial aerosol particles are the main sources of these ice particles. In the precipitating anvils, a trimodal size distribution is prevalent at the upper portion, whereas bimodal or unimodal distributions are more common at the lower levels. The size distributions in the extended anvils exhibit a bimodal shape at the upper levels and a unimodal shape at the lower levels. The properties of the extended anvil compare fairly well with the observational results for one case but not as well for the other two cases. Nevertheless, both the observations and simulations show that smaller particles (diameter < 100 μm) are fractionally more important to the total number concentration and ice water content at higher altitudes in the anvil, whereas larger particles (diameter > 100 μm) are more abundant in the middle to lower sections. Sedimentation sorting plays a significant role in determining the structures and evolution of the cirrus anvils. A sensitivity test indicates that the amount of condensation nuclei in the convective inflow may have a strong influence on the number concentration of ice particles, as well as the structure and lifetime of tropical cirrus anvils.

1. Introduction

Tropical cirrus clouds have a major influence on the global energy budget through their effects on shortwave and longwave radiation [*Liou*, 1986; *Ramanathan and Collins*, 1991]. Numerous studies have demonstrated that these radiative effects are strongly controlled by the microphysical properties of the clouds, such as the ice water path, effective diameter, ice particle shapes and size distribution [e.g., *Platt*, 1989; *Stephens et al.*, 1990; *Takano et al.*, 1992; *Ou and Liou*, 1995]. The spatial and temporal variations of these microphysical properties are important for the calculation of radiative transfer in climate models. Unfortunately, present knowledge of the microphysical and radiative properties of tropical cirrus clouds is still quite poor. Cirrus cloud parameterizations for use in global climate models [e.g., *Heymsfield and Platt*, 1984; *Ebert and Curry*, 1992; *Moss and Johnson*, 1994; *Krueger et al.*, 1995] were developed from observational data for the midlatitude regions, and are thus not necessarily applicable to the tropics. To better understand the climate feedback effects of cirrus clouds, more observations together with numerical simulations of the detailed microphysical structures of cirrus clouds are needed.

Although direct measurements of cirrus microphysics exist [e.g., *Platt et al.*, 1989; *Heymsfield et al.*, 1990], few have been made in anvils forming from deep convections in tropical regions. Among the few, *Griffith et al.* [1980] used data collected by a one-dimensional optical array particle spectrometer during the Global Atmospheric Research Program (GARP) Atlantic Tropical Experiment to derive ice water contents (IWC). They found that there exist large variations in the vertical structures of IWC between cases. The maximum IWC ranged from a few hundredths to a few tenths grams per cubic meter. *Knollenberg et al.* [1982] studied the microphysical properties of Panamanian anvils using a two-dimensional grey imaging probe and an active cavity aerosol spectrometer during the Water Vapor Exchange

Paper number 96JD03513.
0148-0227/97/96JD-03513$09.00

Experiment. They found that large crystals up to 1 mm in size are injected into the stratosphere during cumulonimbus activity, and then return to lower altitudes before evaporating. IWC were of a few thousandths to a few hundreds grams per cubic meter. Bimodal crystal mass distributions were also noticed. Recently, more detailed microphysical measurements have been done by *Knollenberg et al.* [1993] at Darwin, Australia, during the Stratosphere-Troposphere Exchange Project. They measured the size distributions and shapes of ice crystals in the tops of convective anvils using a combination of a two-dimensional grey optical array imaging probe and two light-scattering instruments. Their measurements made in tropical cirrus anvils revealed surprisingly high concentrations of ice crystals that are typically greater than 10000 L^{-1}. The size distributions generally show mass modes at sizes of 20 to 40 μm, with few particles larger than 100 μm when near the cloud top. *Takahashi and Kuhara* [1993] used videosondes to probe the upper convective clouds over Micronesia and obtained images of the precipitation-sized ice particles. They found crystal number concentrations are in the order of tens to 100 L^{-1}, but occasionally up to 1000 L^{-1}.

Among the few numerical studies on the detailed microphysics of cirrus clouds, *Starr and Cox* [1985a] applied a two-dimensional cloud model with parameterized particle size distributions to investigate the role of various physical (e.g., microphysical and radiative) processes involved in the formation and maintenance of thin cirrus clouds. *Sassen and Dodd* [1988], on the other hand, studied the formation of cirrus particles by homogeneous nucleation in uniformly cooled air using a one-dimensional model with a size-resolved microphysical scheme. A similar modeling study was done by *Jensen et al.* [1994a] with vertical wind speeds taken from a mesoscale model. In an attempt to study the ice-forming mechanisms in cirrus clouds, *Heymsfield and Sabin* [1989] developed a parcel model with detailed microphysics. Since a constant updraft speed of 1 m s^{-1} was used, their simulations are not applicable to strong convection. Hence, studies specifically designed for simulating tropical convective anvils and comparing their results with observations are needed.

In this study, three cases of the detailed microphysical structure of tropical anvils are presented by comparing modeling and observational results for the missions conducted during the Central Equatorial Pacific Experiment (CEPEX).

2. Methods

Tropical cumulonimbus systems often show great complexity. To simplify, the convective system is generalized into four sections according to the macroscopic features of each. The first section is the deep convective cell itself, which usually has the coldest cloud top. The outflow of the deep convection is more of a stratiform structure, generally called the anvil cloud. This outflow portion of the cumulonimbus system is classified as either precipitating, extended, or detached. Immediately away from the deep convection is the thick nimbostratus that can be responsible for up to 50% of the total precipitation from the convection system [*Gamache and Houze*, 1983; *Houze and Rappaport*, 1984]. Further downward is the extended anvil without significant precipitation and becoming thinner with distance away from the convection. After the deep convection diminishes, the remaining anvil cloud starts to dissipate but can still persist for a long period of time and is called the detached anvil.

Cirrus clouds often show two-dimensional structures as a result of interactions and feedbacks between dynamic, thermodynamic and radiative processes [*Starr and Cox*, 1985b; *Sassen et al.*, 1989]. However, due to the computational constraints of our complex microphysical scheme, we are limited to using a one-dimensional approach similar to that of *Jensen et al.* [1994a]. Therefore, the model represents approximately a column of the atmosphere that is advected horizontally. Unlike the approach of *Starr and Cox* [1985a] who prescribed the initial thermodynamic and microphysical profiles of the cirrus anvils, the numerical simulations presented here are performed in two steps. Since most of the ice particles entering the anvils originate in the deep convection, it is necessary to model the cumulus convection in order to generate proper initial conditions for the outflow making up the anvil clouds. In the first step, a one-dimensional, time-dependent model simulates the deep convection. The dynamics and initial perturbation schemes used are the same as those of *Wisner et al.* [1972]. A thermal bubble 3 K warmer than the ambient air initiates the convection, and when the simulated convection reaches a quasi-steady state, the convective outflow is isolated and then used as the input for a separate anvil simulation. The effect of condensate loading on the vertical air motion in the deep convection is included. The anvil simulation is also one-dimensional and time-dependent, but without dynamics. Hence, only the effect of condensate loading is considered in determining the vertical air motion. Judging from the macroscopic features, the first 2 hours of the separate anvil simulation is taken to represent the precipitating anvil, the next 4 hours as the extended anvil, and thereafter the detached anvil. Since the dynamics of these simulations are relatively unsophisticated, feedbacks such as dynamics-radiation are not considered.

The detailed cloud microphysical scheme for both the deep convection and the anvil simulations is based on the multicomponent microphysical model of *Chen and Lamb* [1994], which categorizes liquid-phase particles according to their mass, solute content, and shape. A method-of-moments type scheme is used to conserve various physical and chemical properties of cloud particles. Liquid-phase microphysical processes considered in the model are the activation of condensation nuclei into cloud drops, the subsequent condensational growth, and collision-coalescence and breakup. According to *Whitby* [1978], a trimodal distribution of condensation nuclei (CN) for the marine background atmosphere is used as the model input for all cases, with a total number concentration of 400 cm^{-3} at the surface. Ice-phase processes included are heterogeneous deposition nucleation, heterogeneous freezing, contact freezing, homogeneous freezing, diffusional growth, accretional growth, rime-splintering, melting, shedding and aggregation. Following *Chen and Lamb* [1994], the number concentration of ice nuclei that may be active for deposition nucleation or contact nucleation is assumed to be 400 L^{-1} at the surface.

The observational data is obtained from the three sampling missions (March 17, April 1, and April 4, 1993) performed during CEPEX with airborne microphysical measurements in anvils. The data reported here are from the two-dimensional cloud probe (2DC), measuring particles down to about 60 μm in diameter. Sounding data acquired at Nandi, Fiji (17.39 °S, 177.24 °E) on the three sampling dates are used to represent ambient vertical profiles of temperature, pressure and humidity for the three simulations. Details of the measurements and missions during CEPEX can be found in the works of *McFarquhar and Heymsfield* [1996] and *Heymsfield and McFarquhar* [1996].

3. Results

In this section, modeling results for the deep convection and the outflow anvils and observations from the three case studies during CEPEX will be presented. However, since most of the measurements were made away from deep convection, intercomparison between observational and model results will only be given for the outflow anvils. In each case, the vertical profiles of the macroscale properties (i.e., the condensed water content, total number concentration, and effective diameter) and the microscale properties (i.e., the detailed size distributions) will be successively discussed for the convective core, the precipitating anvil, the extended anvil, and the detached anvil.

3.1. Case 1: April 4, 1993

Targeted on a well-defined and persistent thick cirrus anvil, the April 4 case has the best microphysical measurements made during CEPEX. Since significant dissipation did not occur during the mission, and there were only a few particles in a precipitation trail descending below the average cloud base, the April 4 case can be regarded as an early stage of the extended anvil. Hence, comparisons between the simulations and observational results will be focused on the precipitating and extended anvils.

The convective model produced deep convection with a cloud top initially reaching 15 km. After the cloud top overshooting has settled down, the convection reached a quasi-steady state in about 20 min of simulation time, with a cloud top height of 14.5 km and cloud top temperature of 204 K. In comparison, the minimum Geostationary Meteorological Satellite (GMS) brightness temperature for this cloud system was approximately 210 K. A maximum updraft speed of 35.4 m s^{-1} occurs at 9.2 km. As will be discussed in the next section, this maximum updraft speed is probably too high for the tropical region.

Figure 1a shows the number concentration of liquid drops, including interstitial aerosol particles and cloud droplets, as well as ice particles, for the convective core. The drop number concentration (dashed line) decreases with height as a result of air expansion, dilution by mixing, collection by precipitation particles, and freezing. At above 10.5 km, only the interstitial aerosol particles are present as liquid drops. Since the collection of these interstitial particles by ice is rather insignificant, the decrease of their number concentration with height reflects largely the expansion of air. Significant numbers of ice particles (solid line) with a concentration greater than 1 L^{-1} first appear at about 7 km via heterogeneous ice nucleation. This value then increases to a maximum of 870 L^{-1} at 11.2 km, mostly through the freezing of cloud drops. At higher levels, the number concentration decreases down to about 250 L^{-1} near the cloud top. The decrease in number concentration with height for ice particles is somewhat faster than that for interstitial aerosol particles, reflecting the effects of aggregation and sedimentation in addition to air expansion.

Figure 1b shows the quasi-steady state vertical profiles of liquid water and ice water content. The cloud base is about 700 m above sea level as indicated by the sharp increase of condensed water. For the lower part of the cloud, liquid water content (dashed line) increases with height and reaches a maximum of 7 g m^{-3} at 7 km. At higher altitudes, liquid water is converted gradually into ice, resulting in a maximum ice water content (solid line) of 6.2 g m^{-3} at 9.5 km. The total condensed water (dotted line) has a maximum of 7 g m^{-3} occurring at about the same height as that of liquid water.

Figure 1c shows the effective diameter D_{eff} [cf. *McFarquhar and Heymsfield*, 1996] of cloud particles. Above the cloud base, D_{eff} of cloud droplets (dashed curve) increases with height from 20 μm to a maximum of 127 μm at 7.7 km. The D_{eff} of droplets then decreases with height due to the conversion of liquid mass into ice. At above 10.5 km, the D_{eff} is less than 0.01 μm, reflecting the presence of only the very small interstitial aerosol particles. Note that the effective diameter D_{eff} is very sensitive to the existence of larger particles. The relatively large D_{eff} below the cloud base indicates the presence of some large precipitation particles (see Figure 2 for detailed size distributions). The effective diameter of ice particles (solid curve) increases steadily from 220 μm at 6 km to 800 μm at 14.5 km, showing some growth processes occurring at these altitudes. The details of the growth processes will be discussed by examining the evolution of particle size distributions given in Figures 3 and 4.

Figures 2 and 3 show the detailed size distributions of liquid and ice particles as a function of diameter for selected height levels. To simplify the presentation, the size distribution in each panel has been averaged over levels within the indicated height range. Also, the first size category in each panel covers all particles less than 1 μm in diameter, whereas the last category cov-

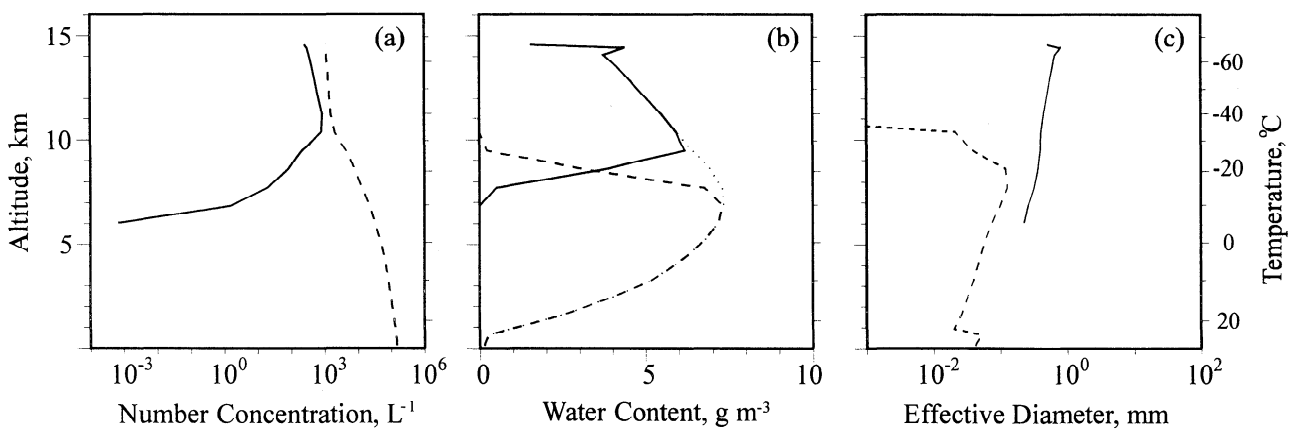

Figure 1. Simulated vertical profiles of (a) number concentration, (b) water content, and (c) effective diameter in the deep convection for the April 4 case. The right axis indicates the temperatures corresponding to the altitude shown at the left.

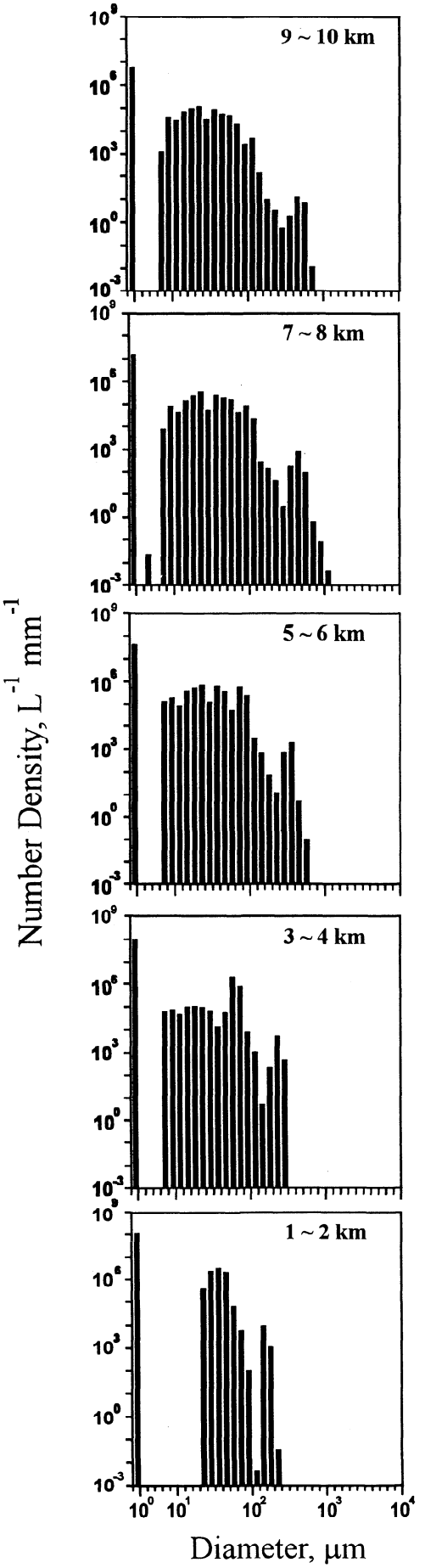

Figure 2. Simulated size distributions of liquid drops at various height levels in the deep convection for the April 4 case. The ordinate is the number density in L^{-1} mm^{-1}, and the abscissa is drop diameter in micrometers.

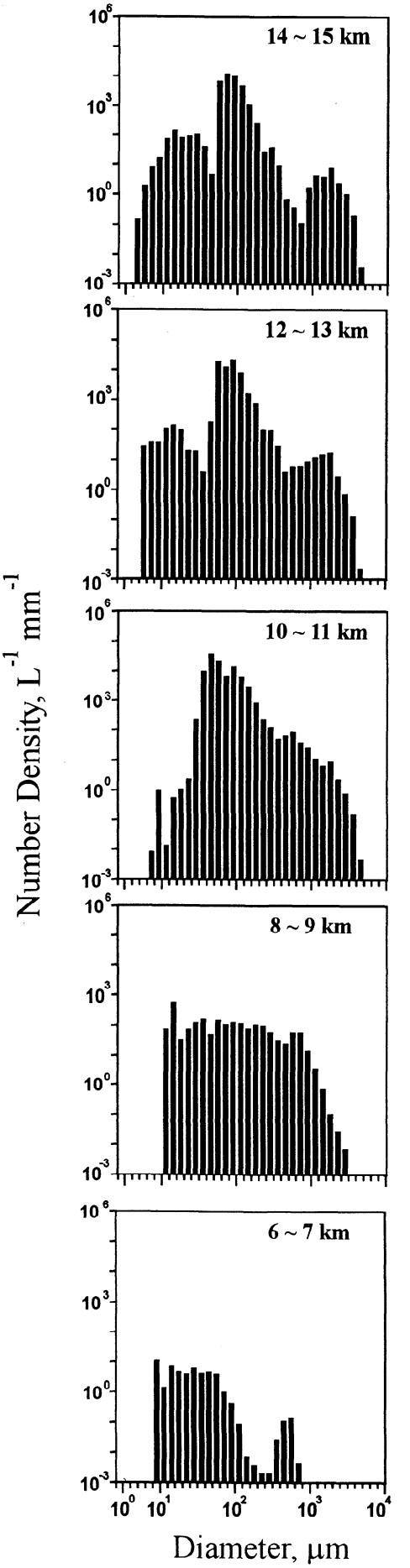

Figure 3. Same as Figure 2, but for ice particles. The ordinate is the number density in L^{-1} mm^{-1} and the abscissa is the maximum dimension in micrometers.

ers all particles larger than 8 mm. The bottom panel (1 ~ 2 km) of Figure 2 is for the size distribution not too far above the cloud base, showing a distinctive gap between the populations of cloud droplets and the interstitial particles (which is in the first size category with diameters $D < 1$ μm). The size distribution of cloud droplets exhibits two modes. The first mode, which has a modal value of about 40 μm, represents the cloud drop population. The second mode, with $D > 100$ μm, represents the precipitation particles formed by coalescence. For heights above 3 km, there exists a population of newly formed cloud drops with smaller sizes (10 μm $< D <$ 40 μm). The existence of these smaller cloud drops is an indication of secondary cloud drop activation [cf. *Paluch and Knight*, 1984; *Chen*, 1994]. However, this mode gradually blends in with the main cloud drop population as the air moves further up. Thus, the cloud drop population appears to be a broad single mode at the higher levels. The drop size spectrum becomes broader as the coalescence process has occurred more at higher levels. At the 7 ~ 8 km level, drops with diameters as large as 1 mm develop. Because of the strong updraft, these particles cannot fall to the cloud base as precipitation particles. So, this simulation can only represent the core region of the convective system, which is a common deficiency of such one-dimensional models. At altitudes higher than 9 km, collection by ice particles becomes appreciable. In addition, as cloud glaciation begins, the saturation ratio in the air eventually becomes subsaturated with respect to water, causing the droplets to evaporate. At temperatures lower than about -30°C, heterogeneous freezing and then homogeneous freezing also become effective. All these processes work together to cause the rapid diminishing of the drop population. As a result, all drops except the interstitial aerosol particles have disappeared above 11 km.

The size distribution of ice particles as a function of their maximum dimension D_m is shown in Figure 3. Ice particles first appeared at the 6 to 7 km levels with a bimodal size spectrum. These two modes represent particles from quite different origins. The model of *Chen and Lamb* [1994] keeps track of the solute content in all cloud particles, so it is possible to judge the origin of ice crystals by checking their solute concentration. The particles in the smaller size mode (centered between 10 and 100 μm) are characterized by solute concentrations less than 0.1 μmol kg^{-1}, indicating that they are mainly vapor-grown crystals. Particles in the larger size mode (centered around 500 μm) have distinctly higher solute concentrations of 10 to 5000 μmol kg^{-1}, which are concentrations typical in cloud droplets. Thus, these large ice particles are mainly rimed ice. At higher levels, the size spectra are broader and show significant amounts of millimeter-sized particles. Riming and aggregation are the mechanisms responsible for the formation of these large particles. Above 10 km, the number of ice particles increases steadily as the cloud drops turn into ice due to heterogeneous and homogeneous freezing. In the top panel, many new ice crystals with sizes less than about 30 μm appear when there are no cloud drops available for freezing. Because of the very low temperatures, even the interstitial aerosol particles start to freeze homogeneously, thus creating a third mode (with $D_m < 30$ μm) in the size spectra.

After the deep convection produces an anvil, the cloud continues to evolve. Figure 4 shows vertical profiles of the total number concentration, condensed water content, and effective diameter in the outflow anvil. The vertical profiles at 1 hour (thick line) and 2 hours (thin line) correspond to the precipitating anvil, the 4 hours (dashed line) and 6 hours (dash-dotted line) profiles correspond to the extended anvil, and the 12 hours profile (dotted line) represents the detached anvil. The glaciation of the outflow anvil occurs rather rapidly such that all cloud droplets disappeared within the first 30 min of the anvil simulation, hence only the properties of ice particles are presented in Figure 4. In the precipitating anvil (thick and thin lines in Figure 4a), the number concentration exceeds 1100 L^{-1} in the upper portions (~ 14 km) of the anvil. Compared with the maximum number concentration of 870 L^{-1} in the convective core (Figure 1a), evidently new ice particles are formed by the freezing of interstitial aerosol particles. Precipitation particles with concentrations of 0.1 to 10 L^{-1} can also be seen below the anvil base (which is at about 10 km), hence justifying the identification of a precipitation anvil. Cloud settling is evident with the progress of time, as can be seen from the lowering of the cloud top. In the extended anvil (dashed and dash-dotted lines), the maximum particle concentrations are still around 1000 L^{-1} but now occur near the bottom of the anvil. On the other hand, the number concentrations at the anvil tops have been reduced to 10 L^{-1}. Essentially no precipitation particle falls below the cloud base at this time. In the detached anvil (dotted line), the cloud sinks down further, with a maximum number concentration of about 400 L^{-1} near the bottom of the cloud. Note that besides the settlement of the particles

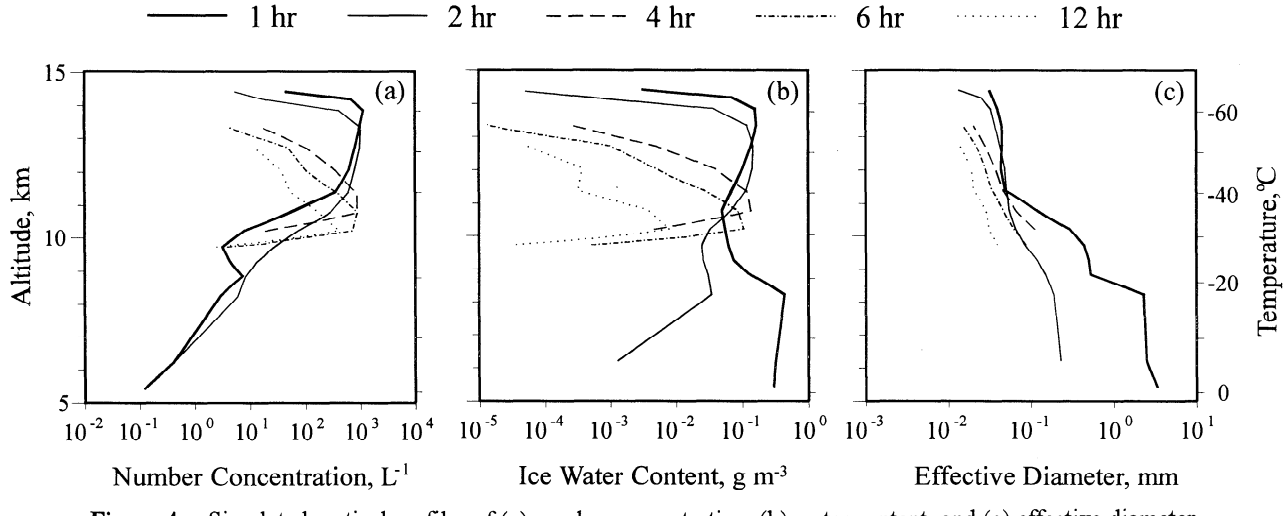

Figure 4. Simulated vertical profiles of (a) number concentration, (b) water content, and (c) effective diameter in the outflow anvil for the April 4 case.

themselves, the only process considered in the model that can cause the cloud layer to move downward is the loading effect. Large-scale subsidence motion, which may also cause ice particles to evaporate and hence reduce the number concentration, is not considered.

To compare with the model results shown in Figure 4, vertical profiles of macroscopic quantities estimated from the microphysical measurements are shown in Figure 5. The observed number concentrations, which are averaged over one flight leg, range from several tens to over 100 L^{-1}, which are less than those from the simulation. However, since the 2-D probes do not accurately measure particles smaller than about 100 μm in diameter, the actual number concentration could be higher. The video particle sampler data [see *McFarquhar and Heymsfield*, 1996] indicate that there exist a significant number of ice particles that may not be detected by the 2DC. In general, the observed data show that the number concentration in the extended anvil decreases with increasing altitude, a trend similar to that in the simulated results.

As shown by the thick and thin solid lines in Figure 4b, the simulated ice water contents for the precipitating anvil have maximums of just over 0.1 g m^{-3} in the upper part of the anvil. The ice water contents below the anvil base are rather high, indicating significant precipitation. In the extended anvil (dashed and dash-dotted lines), ice water content decreases with increasing altitude, with their maximums of about 0.1 g m^{-3} now occurring at the bottom of the anvil. The observational results shown in Figure 5b exhibit a similar trend, with a maximum value of about 0.08 g m^{-3} near the bottom of the anvil. In the detached anvil (dotted line in Figure 4b), the ice water content has a similar profile, but the values are one order of magnitude less than those in the extended anvil. It should be noted that there were substantial variations in the quantities measured by the 2DC occurring over the whole flight leg. However, the trends for the decrease with increasing altitude are clearly seen in the averages.

Figure 4c shows the simulated vertical profiles of the effective diameter D_{eff}. In the precipitating anvil (thick and thin solid lines), D_{eff} ranges from 20 μm at the cloud top to several hundred micrometers near the cloud base. Below the cloud base, which is at about 10 km, millimeter-sized particles are present during the first hour. In the second hour, the D_{eff} decreases to around 100 μm. The large particles at heights below 10 km are characterized by low number densities and high ice water content, which are indications of precipitation particles. The effective diameter generally decreases with time and height. In the extended anvil, D_{eff} is typically about 20 μm at the top and around 100 μm near the bottom. Compared with Figure 5c, the observed D_{eff} shows a similar decreasing trend with increasing altitude and has values ranging from 30 μm near the top to 200 μm at the bottom. Note that these observed values should be somewhat lower if particles smaller than the detection limit are considered. In the detached anvil, D_{eff} decreases to about 15 μm at the top and less than 40 μm at the bottom.

The simulated particle size spectra in the precipitating anvil (averaged over the first hour) and the extended anvil (averaged from 4 to 6 hours) are shown in Figures 6a and 6b, respectively. For comparison, those measured by the 2-D probes are shown in Figure 6c. Since temperature is a common surrogate for height in cirrus parameterization for global models, these figures are presented for temperatures (with corresponding heights given in the opposite vertical ordinate). Note that the height levels for the simulation and observation correspond only roughly. The lower size bins of the model results are shaded to indicate they are not detectable by the 2-D probes. Note that the size resolution for $D_m < 10$ μm is only one half of that for $D_m > 10$ μm.

The top 2 frames in Figure 6a show that the simulated size spectra in the upper part of the precipitating anvil are trimodal. Particles in the first mode (with a modal value of around 10 μm) originate mostly from frozen interstitial haze drops. These drops normally do not freeze until the temperature becomes lower than about -40 °C because of the depression of freezing point by solutes [cf. *Heymsfield and Sabin*, 1989]. Therefore, this mode is not significant at lower levels. Particles of the second mode (with a modal value of about 100 μm) are mostly from frozen cloud drops because they are the expected size and because the number concentrations are too high to be accounted for by other ice nucleation processes. The last mode (with a modal value around 1 mm) is mostly composed of graupel and crystal aggregates. The second and third modes become broader at lower levels, showing the effect of sedimentation sorting. Large, millimeter-sized particles are present throughout the cloud, showing significant precipitation activity. The levels lower than those of the bottom panel are below the cloud base and without a prominent mode in the size distribution.

The number of precipitation-sized particles decreases dramatically at all levels in the extended anvil. As shown in Figure 6b, particles larger than 1 mm are no longer present. The number of smaller particles also decreases because of sedimenta-

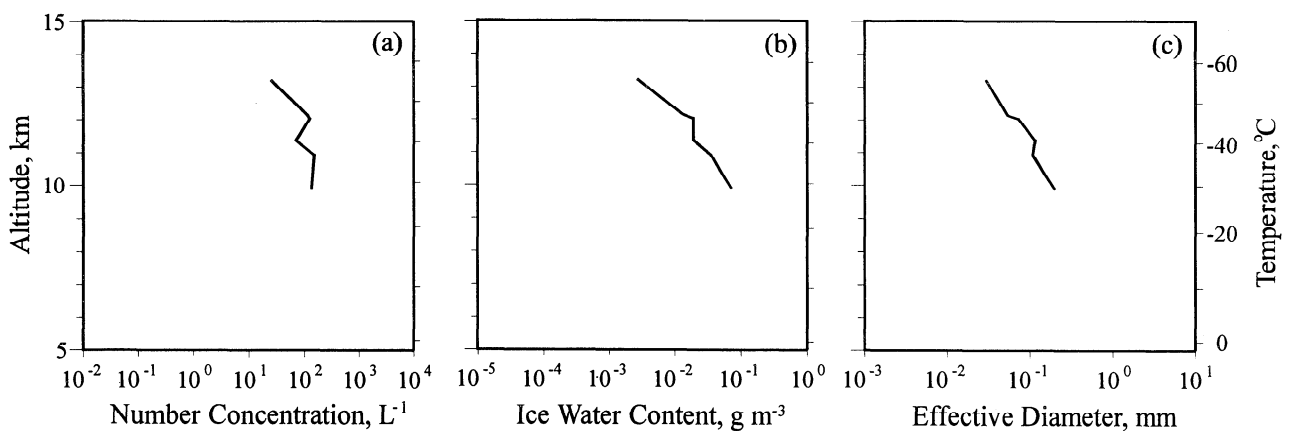

Figure 5. Same as Figure 4, but for the observed results.

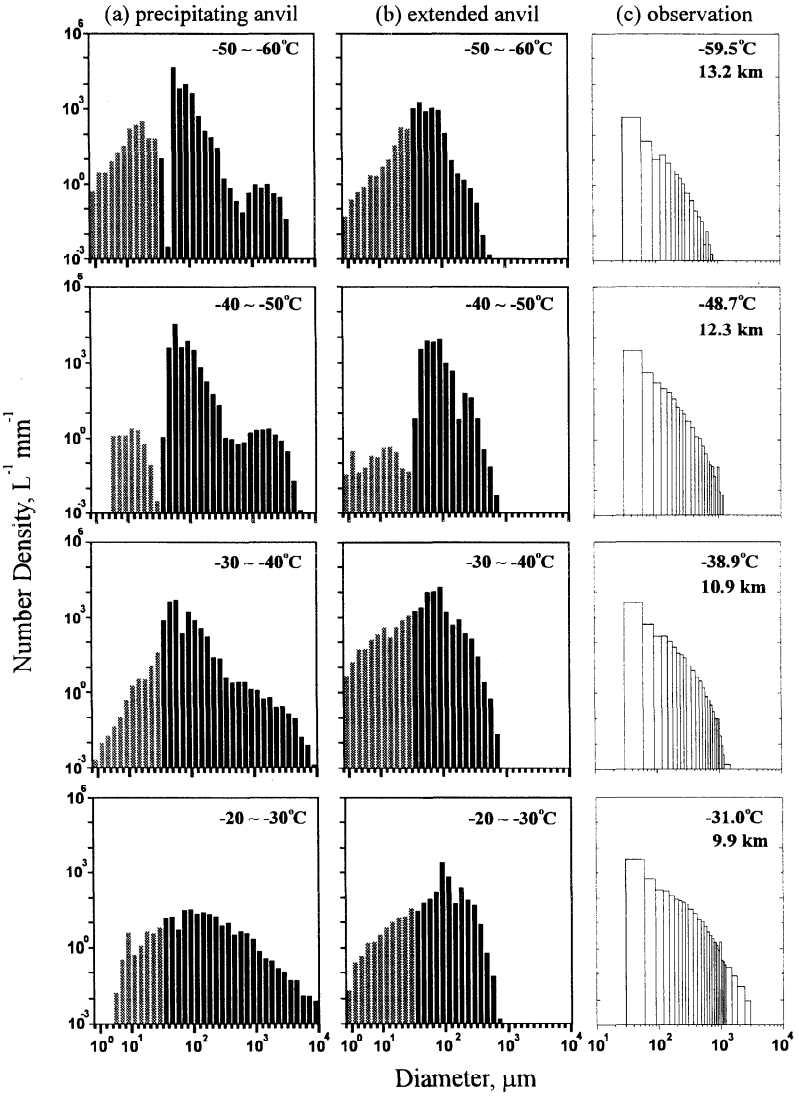

Figure 6. Intercomparison of particle size distributions for the April 4 case, showing (a) simulated precipitating anvil, (b) simulated extended anvil, and (c) observed results. The ordinate is the number density in L^{-1} mm^{-1} and the abscissa is the maximum dimension in micrometers.

tion, aggregation, and evaporation. Thus, the trimodal feature in the upper part of the precipitating anvil is no longer obvious. The most prominent mode occurs at about 100 μm. Such a unimodal spectrum becomes more common with the advance of time, especially at the lower levels. Particles below the cloud base have disappeared almost entirely. Figure 6c shows particle size spectra observed during CEPEX for the April 4 case for four selected levels. Compared with the simulated extended anvil, the observed number distributions are similar in shape and magnitude, with somewhat more large particles and fewer medium size particles. The precipitation mode is not seen in this case. Note that the unimodal shape pertains only to the number distributions. An additional mode would appear at the size of about a few hundred micrometers in both the extended anvil and the observed results if the mass distribution was plotted [*McFarquhar and Heymsfield*, 1996]. The importance of small and medium sized ice particles ($D < 100$ μm) is often neglected in many studies. These particles may contribute significantly to the total number concentrations and even ice water contents especially in the upper anvils, where the particles are generally smaller. Although data from the 2DC do not provide reliable information for particles smaller than about 100 μm, preliminary results from the video ice particle sampler (VIPS) measurements [*McFarquhar and Heymsfield*, 1996] do indicate the existence of a significant number of small particles. The relative importance of small crystals, however, can be highly variable. Nevertheless, the concentrations of the small particles detected by the VIPS are in general higher than the model results. The reason for the discrepancy between the model results and observational data for the smallest particles is still under investigation.

Note that the size spectra shown in Figure 6c are averages for the whole flight leg at each height level. By examining the variation along the flight trajectory, *McFarquhar and Heymsfield* [1996] showed that more large crystals are present as the convective core is approached. Thus, the progress from the precipitating anvil (Figure 6a) to the extended anvil (Figure 6b) does comply with the observed horizontal evolution of the size spectra. Clearly, size sorting has at least some importance in determining the structure of the anvil cloud. This result is also in accordance with the findings of *Starr and Cox* [1985b], who showed in

their numerical experiment that precipitation fallout has important effects on the evolution of cirrus clouds.

The relative importance of large and small particles is shown in the next two figures. Figure 7 shows the simulated number fraction f_N (dashed lines) and mass fraction f_M (solid lines) of particles with diameter smaller than 40 μm (detection limit of 2DC) or 100 μm (accuracy limit of 2DC). In the upper portion of the precipitating anvil (Figure 7a), medium sized particles (40 μm < D < 100 μm) contribute most of the numbers, but about 80% of the total mass is from large particles (D > 100 μm). At the lower portion of the cloud and below cloud base, large particles are fractionally more important in both their number and mass, with 1- f_{N100} > 80% and 1- f_{M100} > 99%, where f_{N100} and f_{M100} are the number and mass fractions of particles with D < 100 μm. Small ice particles (D < 40 μm) are not significant at all levels of the cloud, contributing less than 20% of the total number (f_{N40}) and less than 0.1% of the total mass (f_{M40}, values off the scale). In the extended anvil (Figure 7b), medium-sized particles become dominant in both their number and mass at all levels except near the bottom of the cloud where large particles still contribute more than half of the total mass. Small particles now become more significant, and can account for up to 30% of the total number and 10% of the total mass at the upper portion of the anvil where the ice water content is low. These findings are consistent with the observational results of *McFarquhar and Heymsfield* [1996] in that small particles (D < 40 μm) do not contribute significantly to the total mass except when the ice water content is lower than about 0.001 to 0.01 g m^{-3}. Also, medium sized particles (D < 100 μm) can make a substantial contribution to the total number, total mass, and other physical properties of cirrus anvils.

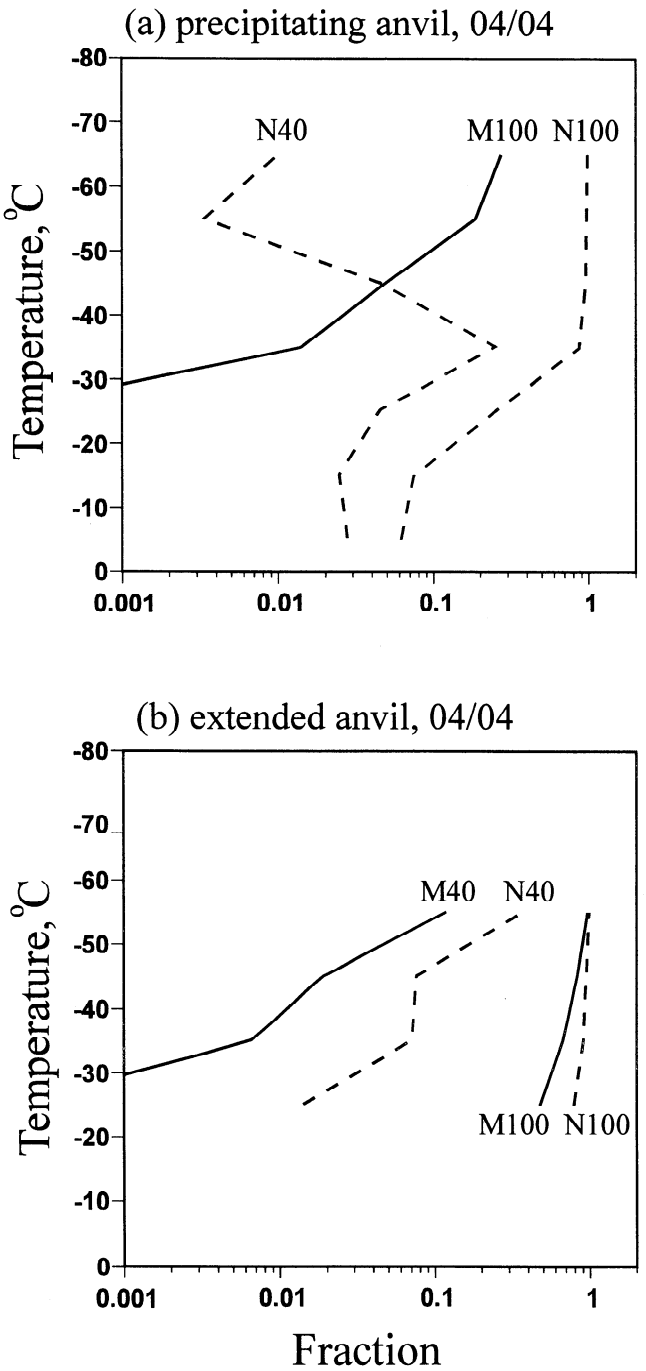

Figure 7. Number (Nx, dashed lines) and mass (Mx, solid lines) fractions of particles with diameters less than x micrometers, where x = 40 or 100, for the April 4 simulation for (a) the precipitating anvil, and (b) the extended anvil. The mass of particles with diameters less than 40 μm in the precipitating anvil is insignificant, so the curve M40 is off the scale.

Figure 8 shows the number median diameter D_N (size cut of 50% total number) and mass median diameter D_M (size cut of 50% total mass). In the precipitating anvil, D_N (thick-dashed line) is 45 μm at the top, 200 μm at the -30° ~ -40°C levels, and > 600 μm at the bottom; whereas D_M (thick solid line) varies from 1.5 mm at the top to over 5 mm at the cloud base. In the extended anvil, D_M (thin solid line) decreases significantly, with values ranging from 65 μm at the top to 130 μm at the bottom. The number median diameter D_N (thin dashed line), however, increases slightly at the upper portion of the cloud, indicating the increased significance of smaller particles. As represented by

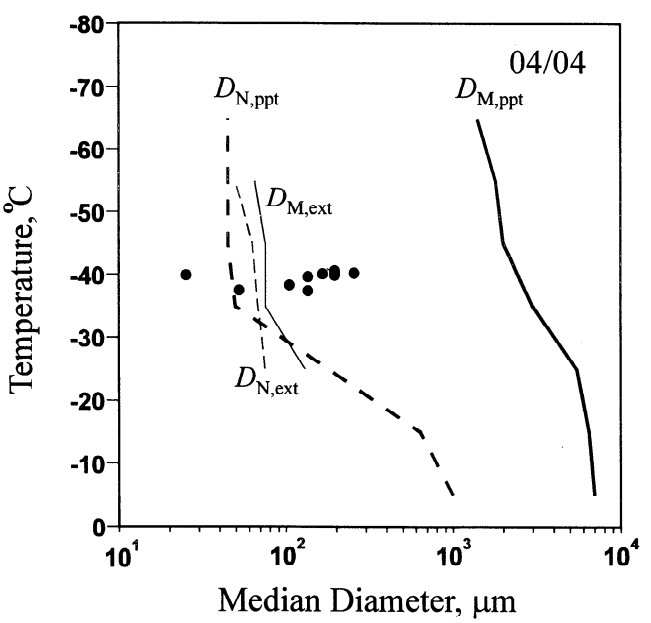

Figure 8. Number median diameter D_N (dashed lines) and mass median diameter D_M (solid lines) of ice particles for the April 4 simulation. In the subscripts of D_N and D_M, "ppt" and "ext" indicate precipitating and extended anvils, respectively. Solid circles are observed mass median diameters from 2DC and VIPS.

the solid circles, a few observed values of D_M currently available for one height level are also included in Figure 8 for comparison. In obtaining these data, a combination of VIPS (for smaller particles) and 2DC (for larger particles) measurements is applied, with 90 μm dividing the two data sets. Although a large variation exists, the observed values lie mostly in between those of the simulated precipitating anvil and extended anvil but much closer to the latter.

The size spectra in the detached anvil are shown in Figure 9. Compared with Figure 6b, the detached anvil has significantly fewer large particles and lower number concentrations than in the extended anvil. The number of particles decreases significantly with increasing height. The size distributions are basically unimodal at all levels. Although most particles are smaller than 100 μm, larger particles can still be found.

In this section, details about the structures of an anvil and the microphysical mechanisms controlling its evolution were discussed. Such detail will not be repeated for the next two cases. Discussions will focus on the macroscale and microscale properties of precipitating and extended anvils and the comparison with observational results. Only brief descriptions will be given for the simulated deep convection.

3.2. Case 2: April 1, 1993

The April 1 case sampled an anvil associated with a dissipating nocturnal thunderstorm. Substantial dissipation occurred during the final legs of the measurements, and hence the observed structure was not as clear as in the previous case. The model simulation produced deep convection reaching a height of 15 km, similar to that in case 1. However, the cloud top temperature is somewhat lower, with a minimum value of 200 K as the convection reached a quasi-steady state. In comparison, the minimum GMS brightness temperature for this system was somewhat less than 210 K.

Figure 10 shows the evolution of the number concentration, water content, and effective diameter of ice particles in the simulated outflow anvils. This anvil differs most significantly from that of case 1 in its greater depth. Also noticeable is the more uniform middle section of the precipitating (1 and 2 hours) and extended anvil (4 and 6 hours). The maximum number concentrations (Figure 10a) and ice water contents (Figure 10b) of the simulated anvil are similar to those in the previous case. Evidently a result of sedimentation sorting, the profiles of the effective diameter again show a decreasing trend in size with decreasing altitudes. Cloud settlement with the progress of time is also obvious. Note that the detached anvil (12 hours from the simulation) appears to leave some residuals at the upper level during the settlement of the cloud. This residual is very low in ice water content and number concentration, with effective diameters less than 10 μm.

The observed vertical profiles shown in Figure 11 exhibit rather large vertical variations. This is caused by the rapid dissipation of the system that occurred during the last couple of hours. The flight penetrations listed in the order in which they were taken are at altitudes of 4.5, 9.9, 12.5, 13.9, 12.0, 11.5, 9.8, 9.2, and 8.5 km. Thus, although measured at almost the same altitude, the number concentrations and ice water contents at the heights of 9.9 km and 9.8 km are rather different. Cloud settlement and evolution are other factors that need to be considered. The maximum number concentration and ice water content are similar to those of the April 4 measurements and are notably lower than the simulated values.

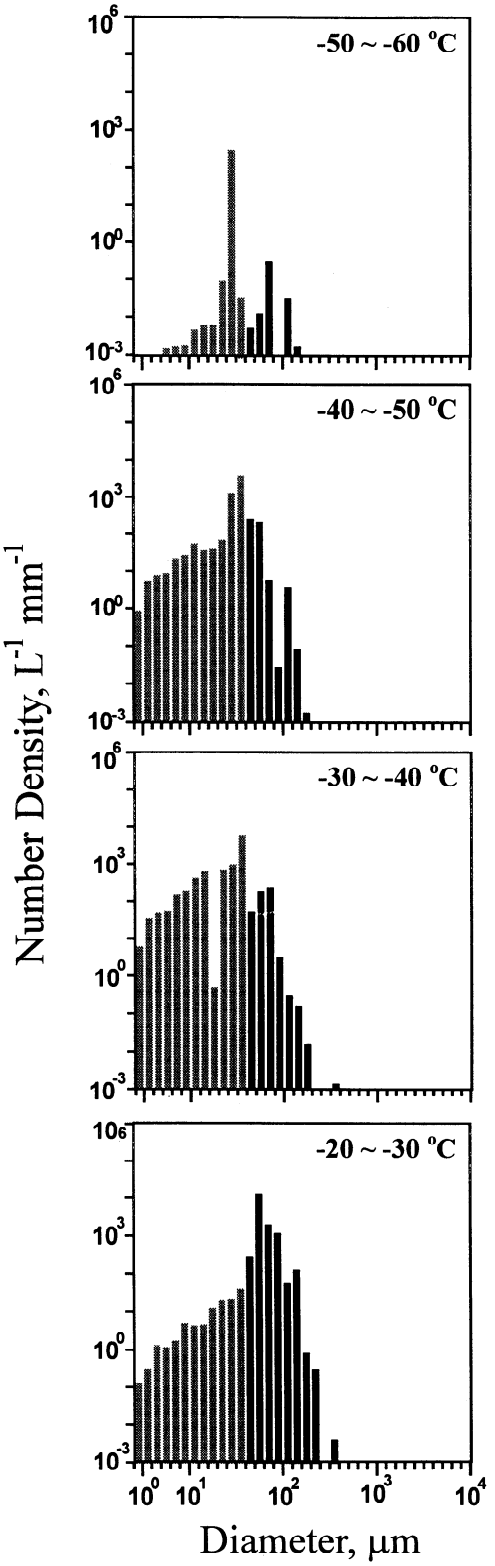

Figure 9. Same as Figure 6a, but for the detached anvil.

Comparisons of the detailed size spectra are shown in Figure 12a for the precipitating anvil, Figure 12b for the extended anvil, and Figure 12c for observational results. The general features of the simulated size distributions are quite similar to those in case 1. At the upper portion of the precipitating anvil, the size spectra still exhibit a trimodal shape, which becomes less prominent at the lower levels. In the extended anvil, the precipitation

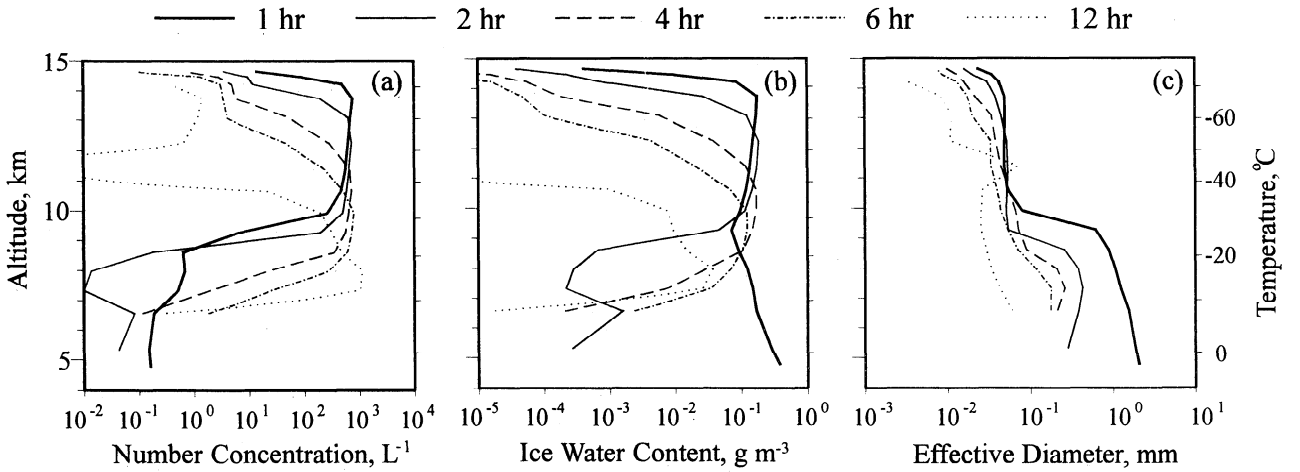

Figure 10. Simulated vertical profiles of (a) number concentration, (b) water content, and (c) effective diameter in the outflow anvil for the April 1 case.

mode is no longer present. The size spectra then appear to be bimodal at higher levels and unimodal at lower levels. Again, shading for $D_m < 40$ μm in Figures 12a and 12b highlights those particles that cannot be detected by the 2-D probes. The observed size spectra at the lower levels reveal some very large particles ($D_m > 1$ mm) that are not present in the extended anvil, but the amounts are much less than those in the precipitating anvil.

The simulated number fractions (f_{N40}, f_{N100}) and mass fractions (f_{M40}, f_{M100}) shown in Figure 13 are quite similar to those in Figure 7 for the April 4 case, except near the cloud top. In the top of the precipitating anvil (Figure 13a), medium sized (40 μm < D_m < 100 μm) particles are now responsible for more than 50% of the total mass, compared with the $f_{M100} - f_{M40} \approx 20\%$ in the previous case. The number fraction of medium sized particles ($f_{N100} - f_{N40}$) is still near 100% in the upper portion of the cloud and much less at the bottom. In the extended anvil (Figure 13b), small particles ($D < 40$ μm) now contribute over 80% of the total number and total mass at the cloud top, compared with $f_{N40} \approx 20\%$ and $f_{M40} \approx 2\%$ in the April 4 case. However, medium sized particles still dominate in both total number and mass at the upper and middle portions of the cloud, whereas large particles dominate at the bottom.

The simulated profiles of median diameters for the April 1 case shown in Figure 14 are quite similar to those of the April 4 case shown in Figure 8, except that $D_{M,ppt}$ at the top of the precipitating anvil is much smaller. The value of $D_{N,ppt}$ (thick-dashed line) varies from 70 μm at the top to > 700 μm at the bottom; whereas $D_{M,ppt}$ (thick solid line) is about 100 μm at the top, then increases rapidly to 2.5 mm in the middle and over 5 mm at the bottom. In the extended anvil, $D_{M,ext}$ (thin solid line) decreases significantly, with values ranging from 35 μm at the top to 350 μm at the bottom. The number median diameter $D_{N,ext}$ (thin dashed line) is slightly smaller than that in the precipitating anvil, with values of 20 μm at the top and 200 μm at the bottom. The observed D_M (solid circles) for two flight legs again show large variations, but the mean values are close to the model results for the extended anvil.

3.3. Case 3: March 17, 1993

A more vigorous convective disturbance with persistent cirrus anvil was sampled on March 17. The simulation produced deep convection reaching a height of 16.5 km (which is 1.5 km greater than that in the previous cases), with a minimum cloud top temperature of 184 K. In comparison, the GMS brightness temperatures for this system show regions of 190 K minimums. The maximum updraft speed in this case is 31 m s^{-1} occurring at the height of 12 km.

Figure 15 shows the evolution of the number concentration, water content, and effective diameter of ice particles in the simu-

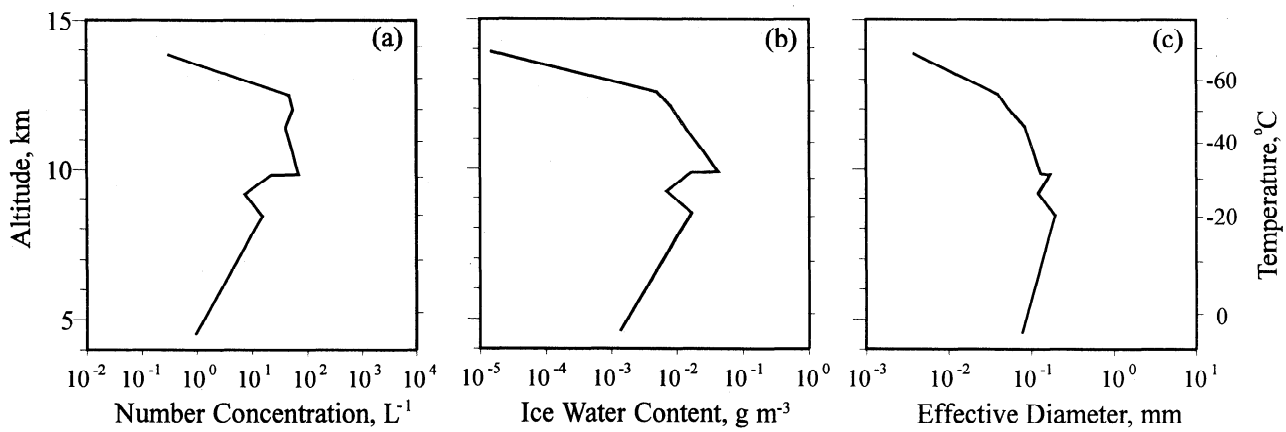

Figure 11. Same as Figure 10, but for the observed results.

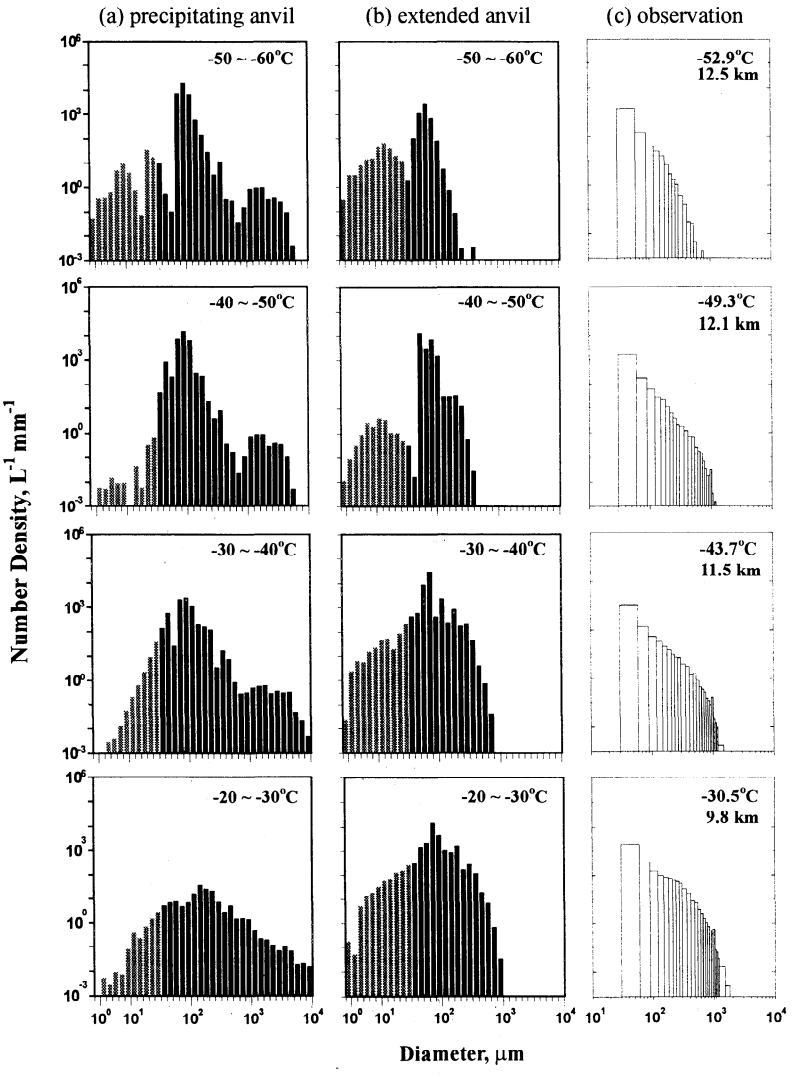

Figure 12. Intercomparison of particle size distributions for the April 1 case for (a) simulated precipitating anvil, (b) simulated extended anvil, and (c) observed results. The units of the coordinates are the same as in Figure 6.

lated outflow anvils. This anvil has the greatest thickness among the three cases. The time evolution clearly shows the settlement of the anvil. Its macroscopic structures are quite similar to those in case 2, with similar maximum number concentrations and ice water contents. However, the observational data (Figure 16) again show lower values. The observed profile of number concentration is rather uniform in the vertical, whereas the simulation shows a maximum in the middle of the anvil. Nevertheless, the simulated and observed effective diameters are similar in magnitude, and both show a decreasing trend with height.

Comparisons of the detailed size spectra are shown in Figure 17a for the precipitating anvil, Figure 17b for the extended anvil, and Figure 17c for observational results. The general features of the simulated anvil differ little from those in the previous cases, with the trimodal distribution in the upper portion of the precipitating anvil and bimodal distribution in the upper portion of the extended anvil. Ample amounts of millimeter-sized particles exist in the precipitating anvil but not in the extended anvil. Marked by the large gap between the two modes, the upper portion of the extended anvil shows clearly two particle populations of different origins. In Figure 17c, the observed size spectra show the existence of some large particles with $D_m > 1$ mm at all levels, indicating the anvil probably was still precipitating. Thus, the observed anvil represents the transition from a precipitating anvil to an extended anvil. Note that measurements for this case were made much closer to the active convection. Unlike the previous cases, the observed size spectra in the upper portion of the anvil are as broad as those at the lower levels. Such a vertical homogeneity is also reflected in the observed vertical profiles shown in Figure 16. However, the simulation failed to catch this phenomenon.

The simulated profiles of number and mass fractions for this case are quite similar to those for the April 1 case (Figure 13). As shown in Figure 18a, median-sized particles contribute most of the total number in the upper part of the precipitating anvil, while large particles dominate in lower levels. However, large particles contribute most to the total mass at all levels, with over 70% at the top and over 99% at the bottom. In the extended anvil (Figure 18b), medium-sized particles contribute to over 90% of the total number and mass at the top of the cloud. Large particles become dominant in mass at the middle portion, but not in

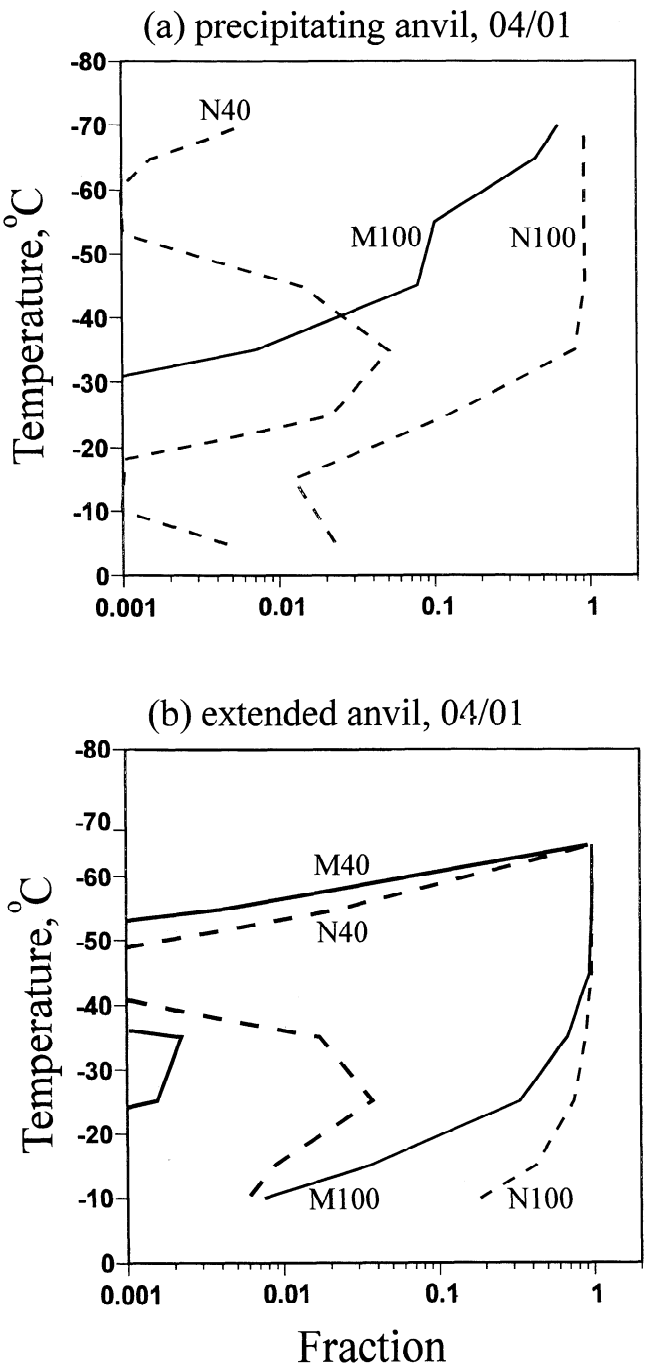

Figure 13. Same as Figure 7, but for the number and mass fractions of the April 1 case.

number until further down near the bottom of the cloud. Small particles are not significant at all levels.

In Figure 19, the simulated profiles of median diameters show only minor variations from those in the April 1 case (Figure 14). The value of $D_{N,ppt}$ varies from 65 μm at the top to > 700 μm at the bottom, whereas $D_{M,ppt}$ is about 300 μm at the top and over 5 mm at the bottom. In the extended anvil, the mass median diameter $D_{M,ext}$ ranges from 55 μm at the top to 400 μm at the bottom, and the number median diameter $D_{N,ext}$ ranges from 35 μm at the top to 300 μm at the bottom. Observational data for D_M are currently not available for this case.

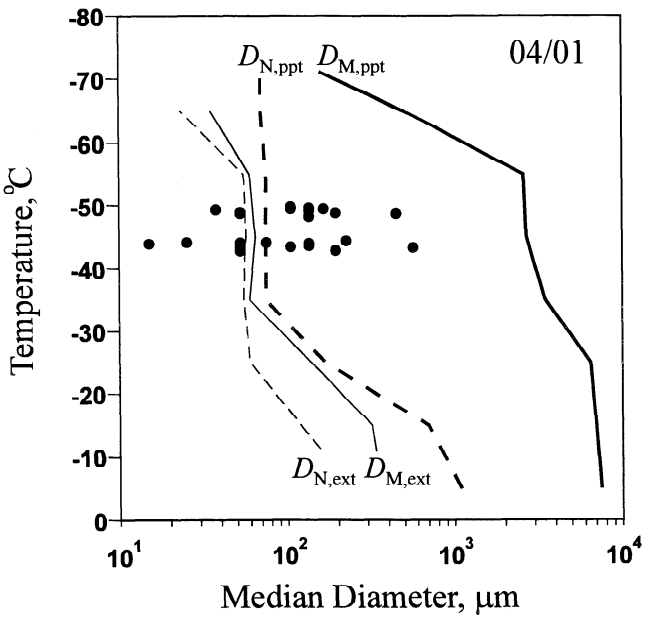

Figure 14. Same as Figure 8, but for the median diameters of the April 1 case.

3.4. Sensitivity Test

In order to see how strongly the number concentration of cirrus ice particles is affected by the number concentration of CN, a sensitivity test is done with 5 times the initial CN for the April 4 case. As shown in Figure 20, the resulting number concentrations of ice particles in the anvil are about 10 times higher than those of the original simulation (cf. Figure 4). Since the majority of the ice particles in the anvil are from frozen drops, an increase in CN leads to an increase in the number of cloud drops and interstitial aerosol particles, and hence the number of ice particles in the anvils. As indicated by the smaller effective diameters shown in Figure 20c, this also lead to a reduction in particle sizes. As a consequence, cloud settling becomes less significant such that the anvil appears to be thicker and lasts longer. In addition, the ice water contents (Figure 20b) are higher than before because of the reduced sedimentation. A large portion of the anvil now appears to be vertically uniform, likely due to the reduced sedimentation-sorting effect. The result shown here is different from that of *Jensen et al.* [1994b], who showed that the number concentration of ice particles in slow-lifting cirrus clouds is not very sensitive to the increase of CN, although in both cases the ice particles form mainly by the freezing mechanism.

The sensitivity test demonstrated that the number concentration of CN has strong effects on the microphysical structure of cirrus anvils. In fact, *Knollenberg et al.* [1993] noticed a possible continental tropospheric influence of CN that might contribute to the high ice number concentrations found during their experiment. Unfortunately, measurement on CN in the convective inflow was not performed during CEPEX. Whether the lack of CN is responsible for the relatively low ice concentrations found during CEPEX requires further investigation.

4. Discussion

The simulations presented in the previous section compared fairly well with observations in one case and not as well in the others. Many factors may contribute to the discrepancies.

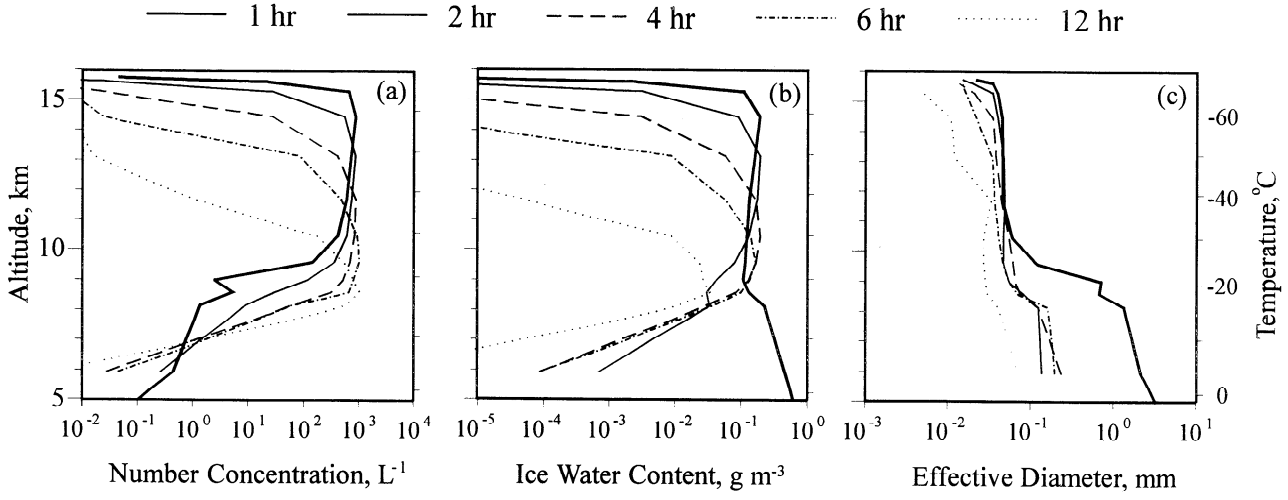

Figure 15. Simulated vertical profiles of (a) number concentration, (b) water content, and (c) effective diameter in the outflow anvil for the March 17 case.

First, the one-dimensional model we applied tends to oversimplify the deep convections that have three-dimensional structures. In addition, the convective activity in cumulonimbus clouds is usually violent and constantly changing. The properties of the convective outflow should thus vary with time. Yet, the anvil simulation takes a snapshot of the convective outflow as its input. Thus, it only represents a Largrangian evolution of a particular cross-section of the anvil. On the other hand, the observational data are collected at different times and places, and often exhibit nonuniform structures that are not captured by the simulations. In addition, large cirrus anvils are sometimes observed to be composed of small-scale convective cells as a result of dynamics-radiation feedback [*Sassen et al.*, 1989]. Such small-scale convections tend to create vertical mixing and may contribute to a vertically more homogeneous anvil (averaged over a certain horizontal distance) like the one in case 3. Other factors that may affect the macroscopic structure of the cirrus anvil are the mesoscale lifting or large-scale subsidence motion [*Lilly*, 1988; *Sassen et al.*, 1989]. These factors are not considered in the simulation, but may provide extra forcing to the growth or decay of the anvil.

Besides the macroscopic features, some discrepancies also exist in the microphysical structures between the simulated and observed results. The maximum particle number concentrations in the anvil for the three simulations are all around 1000 L^{-1}. *Knollenberg et al.* [1993] showed that ice particle number concentrations in tropical cirrus anvils may exceed 1000 L^{-1}. Yet, the observed number concentrations for the three CEPEX cases are significantly lower. *McFarquhar and Heymsfield* [1996] and *Heymsfield and McFarquhar* [1996] discussed several instrumental deficiencies in quantifying the complete size spectra. On the other hand, there exist potential problems with FSSP-type spectrometers used by *Knollenberg et al.* [1993]. Nevertheless, at least for the April 1 and March 17 cases, such large differences in the total number concentration cannot be fully explained by the limitations of instruments. One possible explanation would be the aforementioned subsidence motion that may cause sublimation of the anvil and a reduction in the number concentrations. Significant dissipation was indeed observed during the time of measurements for the April 1 case, but not in the other two cases. Other dynamical and microphysical mechanisms that are not fully considered in the model might have been responsible for the discrepancies.

The mechanisms for the formation of ice particles in tropical cirrus anvils are the condensation-deposition nucleation and contact nucleation at the lower altitudes and the freezing of droplets

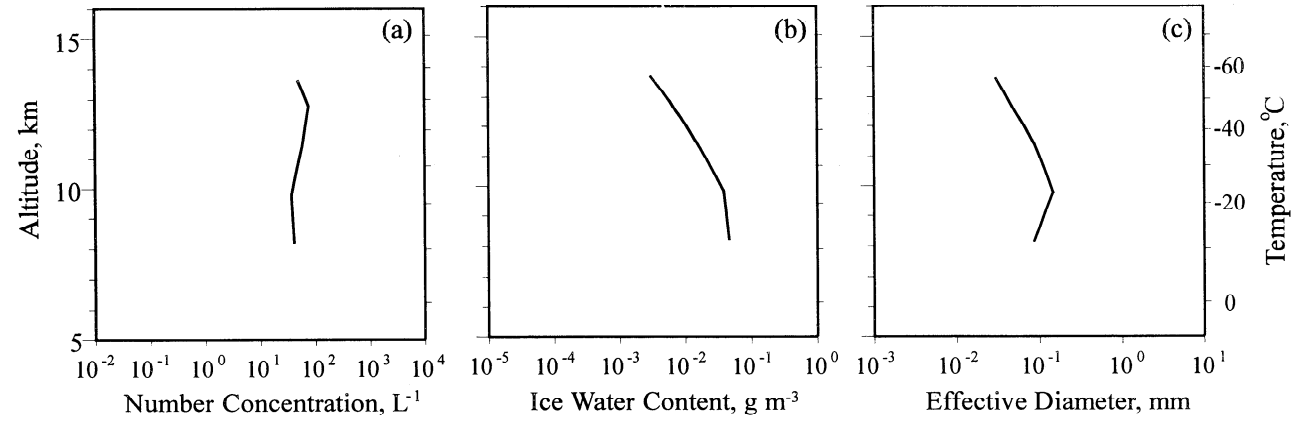

Figure 16. Same as Figure 15, but for the observed results of the March 17 case.

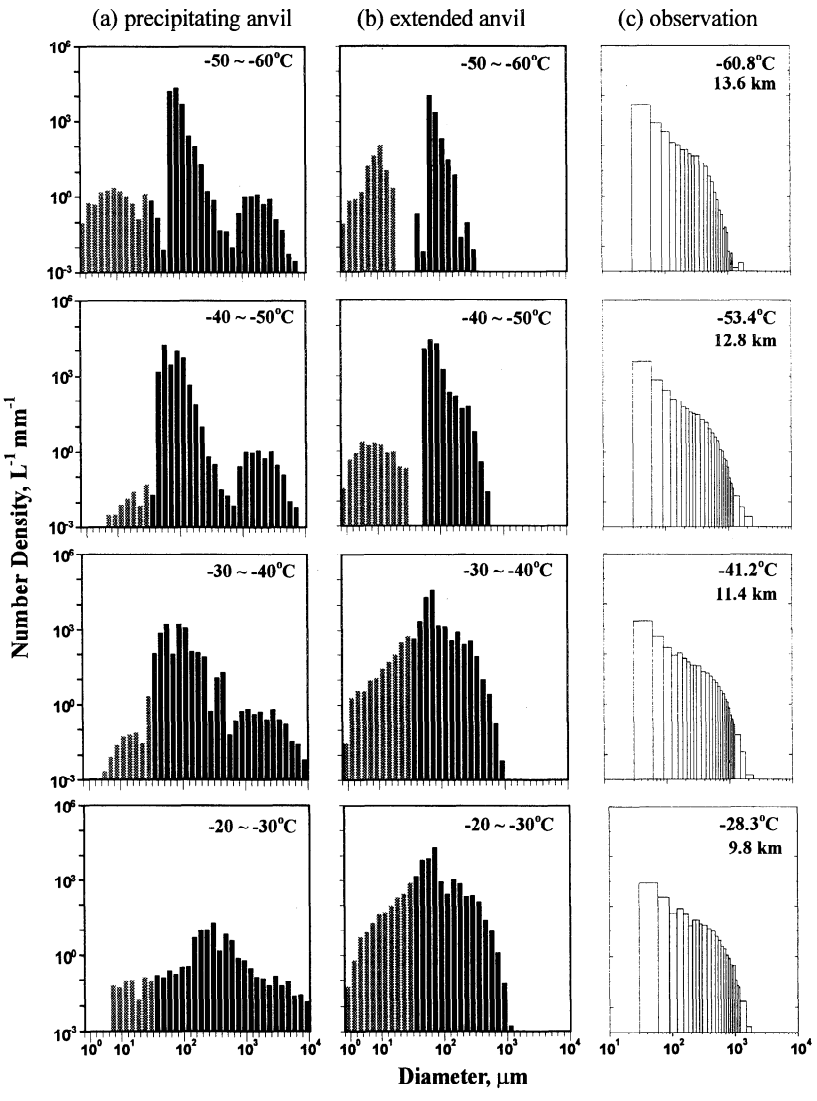

Figure 17. Intercomparison of particle size distributions between the simulated anvils and the observational results for the March 17 case. The ordinate is the number density in L^{-1} mm^{-1} and the abscissa is the maximum dimension in micrometers.

at the upper levels. As mentioned in section 2, the total number of ice nuclei applied in the model is 400 L^{-1} at the surface. Considering the expansion of air and other microphysical effects, these ice nuclei can at best account for about 10% of the 1000 L^{-1} number concentrations obtained in the simulations. Therefore, the main mechanism for the formation of ice particles in the simulated anvils is the freezing of cloud droplets and interstitial aerosol particles. The number concentrations of these cloud droplets and interstitial aerosol particles are directly affected by the initial CN size distribution applied in the model. Thus, as demonstrated by the sensitivity test presented in the previous section, a change in the number concentration of CN can significantly affect the structures of cirrus anvils. Although the CN size distribution normally has large spatial and temporal variations, we applied the same size distribution for all cases due to a lack of in situ measurements, which is another important factor that may affect the model results.

With other initial conditions being equal, the differences between the three simulations are mainly due to variations in the sounding profiles that determine the atmospheric stability and the dynamic structure of the convection. Since cloud drop activation and ice nucleation processes have a strong dependence on the degree of supersaturation, which in turn depends on the updraft speeds, the dynamic structure of the cloud certainly has strong influences on the number concentrations of various cloud particles [*Ochs*, 1978; *Chen*, 1994]. Yet, one-dimensional models, such as the one applied here, can only account crudely for dynamics, especially in the presence of shearing winds and strong interaction with the environment [*Reuter and Yau*, 1987; *Ćurić and Janc*, 1993]. For instance, the updrafts in the three case simulations have maximums of 25 to 35 m s^{-1}. These magnitudes could be too high for the tropical region. Although severe midlatitude cumulonimbi over land frequently develop updrafts over 40 m s^{-1} [*Musil et al.*, 1986; *Miller et al.*, 1988], updrafts in cumulonimbi near the tropical region are normally lower. The highest maximum updraft speeds found off the west coast of Africa during the GARP Atlantic Tropical Experiment [*LeMone and Zipser*, 1980], in the vicinity of the Indian subcontinent during the Summer Monsoon Experiment [*Gamache*, 1990], over the western Pacific warm pool during the Equatorial

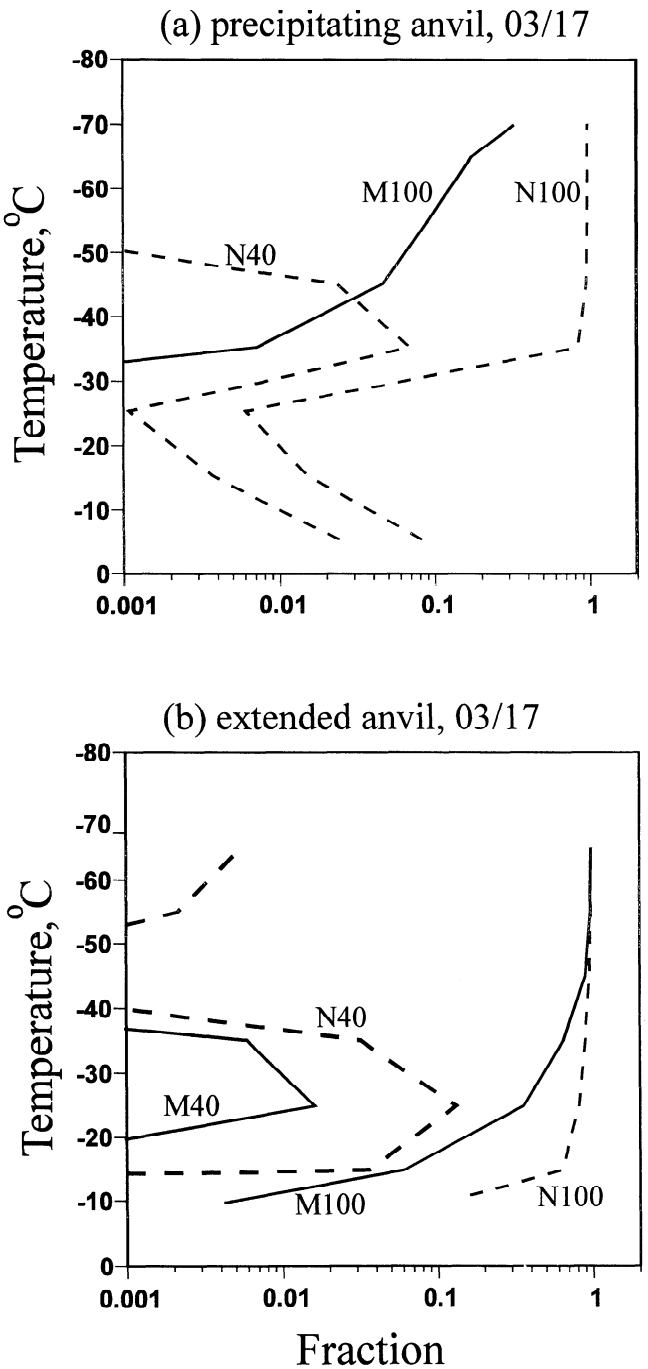

Figure 18. Same as Figure 7, but for the number and mass fractions of the March 16 case.

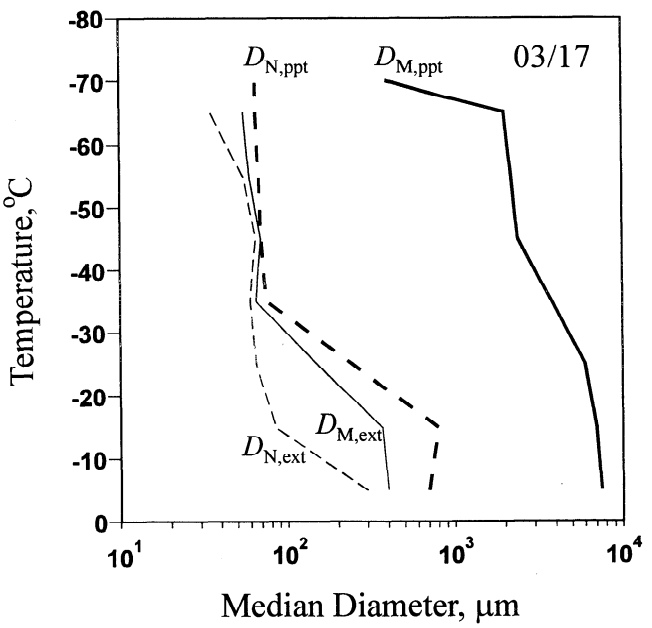

Figure 19. Same as Figure 8, but for the median diameters of the March 16 case.

Mesoscale Experiment [*Lucas et al.*, 1994], as well as in the subtropical ocean southeast of Taiwan during the Taiwan Area Mesoscale Experiment [*Jorgenson and LeMone*, 1989; *Jorgenson et al.*, 1991] are all between 10 to 15 m s^{-1}. Only the measurements made during the Florida Area Cumulus Experiment for the southern Florida region occasionally show comparable maximum speeds of over 30 m s^{-1} [*Wiggert et al.*, 1982], which, however, might be under continental influences. Unfortunately, no verification is available from the CEPEX area. Besides the inherent limitation of the one-dimensional model, the initialization of convection with a thermal bubble 3 K warmer than the ambient air might also influence the model outcomes. A test with a 2 K thermal bubble produced similar updraft profiles in two cases, and failed to develop mature convection in the other. Thus, there is no clear indication that the extra buoyancy from the thermal bubble is the cause of the strong updrafts. Due to the high computational demands of the microphysical scheme, we are limited to using the one-dimensional model at this stage. Considering all the limitations discussed above, the results demonstrated here should only be regarded as a means of assessing the relative importance of various microphysical mechanisms under simplified conditions.

5. Conclusions

By using a one-dimensional microphysical model, the detailed microphysical structures of tropical cirrus anvils are simulated and compared with observations for three cases during CEPEX. The convective system is partitioned into four sections (the deep convection, precipitating anvil, extended anvil, and detached anvil) according to its macroscopic characteristics. The three simulated deep convections, with cloud tops reaching over 15 km, are characterized by strong updrafts and high liquid and ice water contents over 6 g m^{-3}. Conversion of the liquid water into ice occurred between the -30°C and -40°C levels, producing a vast amount of ice particles that are then carried by the convective outflow into the cirrus anvils. The earlier stage of the outflow anvils, i.e. the precipitating anvil, is characterized by ice water contents of several tenths of a gram per cubic meter and abundant precipitation particles below cloud base, which gradually vanish in the extended anvil stage. The macroscopic features of the extended anvil from the simulations correspond fairly well with observations for the April 4 case. However, disagreements in the macroscopic features are more significant for the other two cases.

The microphysical structures of the tropical cirrus anvils are simulated in detail, with the important results summarized as follows.

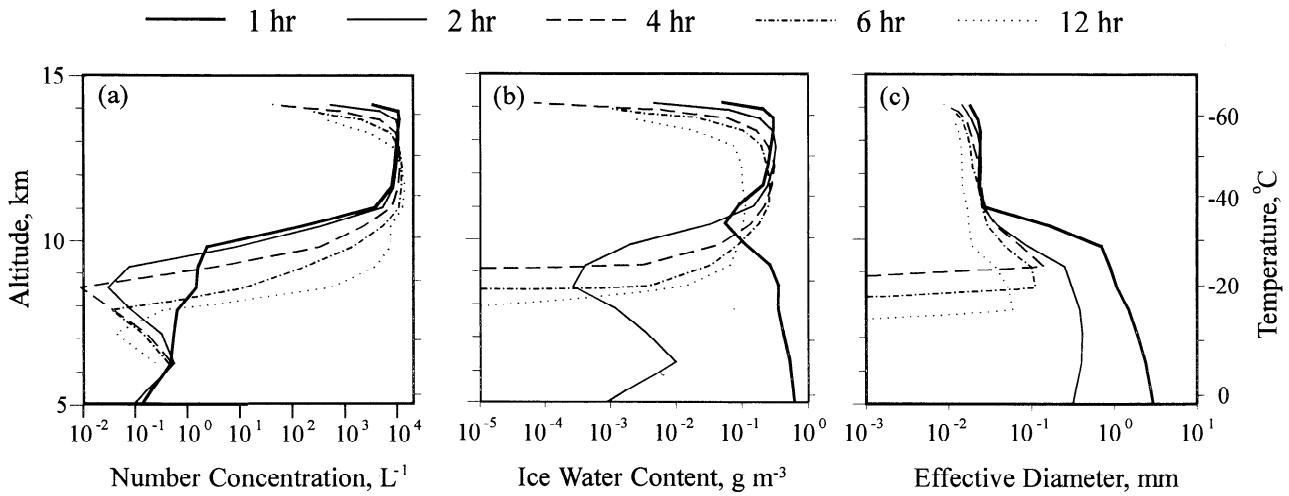

Figure 20. Simulated vertical profiles of (a) number concentration, (b) water content, and (c) effective diameter in the outflow anvil for the April 4 sensitivity test.

1. Ice particles with number concentrations as high as 1000 L^{-1} are present in the precipitating and extended anvils. These ice particles are mostly formed by the freezing of cloud droplets and interstitial aerosol particles.

2. Trimodal size distributions are prevalent in the upper portion of the precipitating anvil with temperatures below about -40°C. The smallest particles, with a modal value around 10 μm, originate mainly from frozen interstitial aerosol particles; the medium sized particles, with a modal value around 100 μm, are mainly from frozen cloud drops; whereas the largest (precipitation sized) particles with a modal value around 1 mm are mainly from crystal aggregates and rimed ice.

3. Size sorting could be important in controlling the vertical structure and time evolution of cirrus anvils. Significantly more large particles exist in the lower portion of the precipitating anvil, where the particle size spectra are typically broader and bimodal or unimodal in shape. Millimeter-sized particles are not present in the extended anvil due to earlier fallout. The total number concentration, ice water content, and effective diameter in the extended anvil generally show a decreasing trend with altitude.

4. Smaller ice particles (D < 100 μm) are fractionally more important in number at the upper part of the anvil, while larger particles are more abundant at the lower levels of the precipitating anvil. For the total mass, large particles with D > 100 μm contribute more in almost all levels of the precipitating anvil. Smaller particles become more important in the extended anvils. They dominate both the total number and mass at the upper part of the cloud, as well as the total number at the lower part of the cloud. Larger particles, however, still contribute more in total mass near the cloud base.

5. A sensitivity test demonstrated that an increase in the number concentration of condensation nuclei can dramatically enhance the number of ice particles in the anvil. The change in number concentrations also affects the vertical structures and the lifetime of cirrus anvils.

Similar to the macroscopic properties, the microscopic features of the simulated anvils also correspond fairly well to observations for the April 4 case, but not as well for the other two cases. The discrepancies in the macroscopic and microscopic properties between the simulations and observations may have resulted from (1) the simplicity of the one-dimensional model, and a lack of dynamic/radiative feedbacks; (2) the inability to describe the large-scale subsidence and small-scale turbulent motions; (3) the inadequacy of the initial conditions such as the CN size distributions; (4) the limitations of observation and instrumentation, and (5) inconsistency in the time of observations.

This study presents some results that may contribute to the understanding of the spatial and temporal evolution of tropical cirrus anvils. Further studies are nevertheless needed in order to have a comprehensive understanding of their general characteristics and effects on climate. For instance, measurement of the number concentration of CN in the convective inflow is important in establishing its relationship with the number concentration of ice particles in the outflow anvils. The relative significance of small particles requires further investigation in order to understand their importance in cloud radiation. In addition, the shapes of ice crystals and their effects on cirrus cloud microphysics and radiative properties are important topics that are not discussed in this study. Further numerical and observational studies are needed to examine the nonlinear interactions between cloud dynamics and radiation. Finally, a study such as this may help in developing cirrus parameterization that is appropriate to the tropical regions.

Acknowledgments. This research is supported under NSC grant 85-2111-M-002-006 and NSF grant ATM-9405024. We are indebted to the Aeromet crew (R. Harris-Hobbs, D. Rusk, R. Wallin, and B. Jones) whose tireless work provided us with these measurements.

References

Chen, J. P., Predictions of saturation ratio for cloud microphysical models, *J. Atmos. Sci., 51*, 1332-1338, 1994.

Chen, J. P., and D. Lamb, Simulation of cloud microphysical and chemical processes using a multicomponent framework, I, Description of the microphysical model, *J. Atmos. Sci., 51*, 2613-2630, 1994.

Ćurić, M., and D. Janc, Predictive capabilities of a one-dimensional convective cloud model with forced lifting and a new entrainment formulation, *J. Appl. Meteorol., 32*, 1733-1740, 1993.

Ebert, E. E., and J. A. Curry, A parameterization of ice cloud optical properties for climate models, *J. Geophys. Res., 97*, 3831-3836, 1992.

Gamache, J. F., Microphysical observations in summer MONEX convective and stratiform clouds, *Mon. Weather Rev., 118*, 1238-1249, 1990.

Gamache, J. F., and R. A. Houze, Water budget of a mesoscale convective system in the tropics, *J. Atmos. Sci., 40*, 1835-1850, 1983.

Griffith, K. T., S. K. Cox, and R. G. Knollenberg, Infrared radiative properties of tropical cirrus clouds inferred from aircraft measurements, *J. Atmos. Sci., 37*, 1077-1087, 1980.

Heymsfield, A. J., and G. M. McFarquhar, A dedicated cloud microphysics mission during the Central Equatorial Pacific Experiment (CEPEX), paper presented at the Eighth Conference on Atmospheric Radiation, Am. Meteorol. Soc., Nashville, Tenn., 1994.

Heymsfield, A. J., and G. M. McFarquhar, High albedos of cirrus in the tropical Pacific warm pool: Microphysical interpretations from CEPEX and from Kwajalein, Marshall Islands, *J. Atmos. Sci., 53*, 2424-2451, 1996.

Heymsfield, A. J., and C. M. R. Platt, A parameterization of the particle size spectrum of ice clouds in terms of the ambient temperature and the ice water content, *J. Atmos. Sci., 41*, 846-855, 1984.

Heymsfield, A. J., K. M. Miller, and J. D. Spinhirne, The 27-28 October 1986 FIRE IFO cirrus case study: Cloud microstructure, *Mon. Weather Rev., 118*, 2313-2328, 1990.

Heymsfield, A. J., and R. M. Sabin, Cirrus crystal nucleation by homogeneous freezing of solution droplets, *J. Atmos. Sci., 46*, 2252-2264, 1989.

Houze, R. A., and E. N. Rappaport, Air motions and precipitation structure of an early summer squall line over the eastern tropical Atlantic, *J. Atmos. Sci., 41*, 553-574, 1984.

Jensen, E. J., O. B. Toon, D. L. Westphal, S. Kinne and A. J. Heymsfield, Microphysical modeling of cirrus, 1, Comparison with 1986 FIRE IFO measurements, *J. Geophys. Res., 99*, 10421-10442, 1994a.

Jensen, E. J., O. B. Toon, D. L. Westphal, S. Kinne and A. J. Heymsfield, Microphysical modeling of cirrus, 2, Sensitivity studies, *J. Geophys. Res., 99*, 10443-10454, 1994b.

Jorgenson, D. P., and M. A. LeMone, Vertical velocity characteristics of oceanic convection, *J. Atmos. Sci., 46*, 621-640, 1989.

Jorgenson, D. P., M. A. LeMone, and B. J.-D. Jou, Precipitation and kinematic structure of an oceanic mesoscale convective system, I, Convective line structure, *Mon. Weather Rev., 119*, 2608-2637, 1991.

Knollenberg, R. G., A. J. Dascher, and D. Huffman, Measurements of the aerosol and ice crystal populations in tropical stratospheric cumulonimbus anvils, *Geophys. Res. Lett., 9*, 613-616, 1982.

Knollenberg, R. G., K. Kelly, and J. C. Wilson, Measurements of high number densities of ice crystals in the tops of tropical cumulonimbus, *J. Geophys. Res., 98*, 8639-8664, 1993.

Krueger, S. K., Q. Fu, and K. N. Liou, Improvements of an ice-phase microphysics parameterization for use in numerical simulations of tropical convection, *J. Appl. Meteorol., 34*, 282-287, 1995.

LeMone, M. A., and E. J. Zipser, Cumulonimbus vertical velocity events in GATE, I, Diameter, intensity and mass flux, *J. Atmos. Sci., 37*, 2444-2457, 1980.

Lilly, D. K., Cirrus outflow dynamics, *J. Atmos. Sci., 45*, 1594-1605, 1988.

Liou, K.-N., Influence of cirrus clouds on weather and climate processes: A global perspective, *Mon. Weather Rev., 114*, 1167-1199, 1986.

Lucas, C., E. J. Zipser, and M. A. LeMone, Vertical velocity in oceanic convection off tropical Australia, *J. Atmos. Sci., 51*, 3183-3193, 1994.

McFarquhar, G. M., and A. J. Heymsfield, Cloud particle and thermodynamic measurements of cirrus anvil tops during the Central Equatorial Pacific Experiment (CEPEX), paper presented at the Sixth Conference on Climate Variations, Am. Meteorol. Soc., Nashville, Tenn., 1994.

McFarquhar, G. M., and A. J. Heymsfield, Microphysical characteristics of three anvils sampled during the Central Equatorial Pacific Experiment, *J. Atmos. Sci., 53*, 2401-2423, 1996.

McFarquhar, G. M., A. J. Heymsfield, and J. P. Chen, Three dedicated microphysics missions during CEPEX: Observations and numerical simulations, paper presented at the Symposium on the Regulation of Sea Surface Temperatures and Warming of the Tropical Ocean-Atmosphere System, Am. Meteorol. Soc., Dallas, Tex., 1995.

Miller, L. J., J. D. Tuttle, and C. K. Knight, Airflow and hail growth in a severe northern High Plans supercell, *J. Atmos. Sci., 45*, 736-762, 1988.

Moss, S. J., and D. W. Johnson, Aircraft measurements to validate and improve numerical model parameterizations of ice to water ratios in clouds, *Atmos. Res., 34*, 1-25, 1994.

Musil, D. J., A. J. Heymsfield, and P. L. Smith, Microphysical characteristics of a well-developed weak echo region in a High Planes supercell thunderstorm, *J. Clim. Appl. Meteorol., 25*, 1037-1051, 1986.

Ochs, H. T., III, Moment-conserving techniques for warm cloud microphysical computations, II, Model testing and results, *J. Atmos. Sci., 35*, 1959-1973, 1978.

Ou, S.-C., and K.-N. Liou, Ice microphysics and climate temperature feedback, *Atmos. Res., 35*, 127-138, 1995.

Paluch, I. R., and C. A. Knight, Mixing and the evolution of cloud droplet size spectrum in a vigorous continental cumulus, *J. Atmos. Sci., 41*, 1801-1815, 1984.

Platt, C. M. R., The role of cloud microphysics in high-cloud feedback effects on climate change, *Nature, 341*, 428-429, 1989.

Platt, C. M. R., J. D. Spinhirne, and W. D. Hart, Optical and microphysical properties of a cold cirrus cloud: Evidence for region of small ice particles, *J. Geophys. Res., 94*, 11151-11164, 1989.

Ramanathan, V., and W. Collins, Thermodynamic regulation of ocean warming by cirrus clouds deduced from observations of the 1987 El Nino, *Nature, 357*, 24-32, 1991.

Reuter, G. W., and M. K. Yau, Mixing mechanisms in cumulus congestus clouds, II, Numerical simulations, *J. Atmos. Sci., 44*, 798-827, 1987.

Sassen, K., and G. C. Dodd, Homogeneous nucleation rate for highly supercooled cirrus cloud droplets, *J. Atmos. Sci., 45*, 1357-1369, 1988.

Sassen, K., D. O. Starr, and T. Uttal, Mesoscale and microscale structure of cirrus clouds: Three case studies, *J. Atmos. Sci., 46*, 371-396, 1989.

Starr, D. O., and S. K. Cox, Cirrus clouds, I, A cirrus cloud model, *J. Atmos. Sci., 42*, 2663-2681, 1985a.

Starr, D. O., and S. K. Cox, Cirrus clouds, II, Numerical experiments on the formation and maintenance of cirrus, *J. Atmos. Sci., 42*, 2682-2694, 1985b.

Stephens, G. L., S.-C. Tsay, P. W. Stackhouse, Jr., and P. J. Flatau, The relevance of the microphysical and radiative properties of cirrus clouds to climate and climate feedback, *J. Atmos. Sci., 47*, 1742-1753, 1990.

Takahashi and Kuhara, Precipitation mechanisms of cumulonimbus clouds at Pohnpei, Micronesia, *J. Meteor. Soc. Japan, 71*, 21-31, 1993.

Takano, Y., K.-N. Liou, and P. Minnis, The effects of small ice crystals on cirrus infrared radiative properties, *J. Atmos. Sci., 49*, 1487-1493, 1992.

Whitby, K. T., The physical characteristics of sulfur aerosols, *Atmos. Environ., 12*, 135-159, 1978.

Wiggert, V., R. I. Sax, and R. L. Holle, On the modification potential of Illinois summertime convective clouds, with comparisons to Florida and FACE observations, *J. Appl. Meteorol., 21*, 1293-1322, 1982.

Wisner, C., H. D. Orville, and C. Myers, A numerical model of a hail-bearing cloud, *J. Atmos. Sci., 29*, 1160-1180, 1972.

J.P. Chen, Department of Atmospheric Sciences, National Taiwan University, No. 61, Ln. 144, Sec. 4, Keelung Road, Taipei, Taiwan, Republic of China. (e-mail: jpchen@water.as.ntu.edu.tw)

A.J. Heymsfield and G.M. McFarquhar, National Center for Atmospheric Research, Boulder, CO.

V. Ramanathan, Center for Clouds, Chemistry and Climate, Scripps Institution of Oceanography, La Jolla, CA.

(Received August 16, 1996; accepted November 1, 1996.)